



MTE-NODDI: Multi-TE NODDI for disentangling non-T2-weighted signal fractions from compartment-specific T2 relaxation times

Ting Gong^{a,b}, Qiqi Tong^a, Hongjian He^{a,*}, Yi Sun^c, Jianhui Zhong^{a,d,**}, Hui Zhang^b

^a Center for Brain Imaging Science and Technology, College of Biomedical Engineering and Instrumental Science, Zhejiang University, Hangzhou, China

^b Department of Computer Science & Centre for Medical Image Computing, University College London, UK

^c MR Collaboration, Siemens Healthcare, Shanghai, China

^d Department of Imaging Sciences, University of Rochester, Rochester, NY, United States

ARTICLE INFO

Keywords:

Diffusion MRI
NODDI
T2 relaxation
Brain development
Brain maturation
Aging

ABSTRACT

Neurite orientation dispersion and density imaging (NODDI) has become a popular diffusion MRI technique for investigating microstructural alternations during brain development, maturation and aging in health and disease. However, the NODDI model of diffusion does not explicitly account for compartment-specific T2 relaxation and its model parameters are usually estimated from data acquired with a single echo time (TE). Thus, the NODDI-derived measures, such as the intra-neurite signal fraction, also known as the neurite density index, could be T2-weighted and TE-dependent. This may confound the interpretation of studies as one cannot disentangle differences in diffusion from those in T2 relaxation. To address this challenge, we propose a multi-TE NODDI (MTE-NODDI) technique, inspired by recent studies exploiting the synergy between diffusion and T2 relaxation. MTE-NODDI could give robust estimates of the non-T2-weighted signal fractions and compartment-specific T2 values, as demonstrated by both simulation and *in vivo* data experiments. Results showed that the estimated non-T2 weighted intra-neurite fraction and compartment-specific T2 values in white matter were consistent with previous studies. The T2-weighted intra-neurite fractions from the original NODDI were found to be overestimated compared to their non-T2-weighted estimates; the overestimation increases with TE, consistent with the reported intra-neurite T2 being larger than extra-neurite T2. Finally, the inclusion of the free water compartment reduces the estimation error in intra-neurite T2 in the presence of cerebrospinal fluid contamination. With the ability to disentangle non-T2-weighted signal fractions from compartment-specific T2 relaxation, MTE-NODDI could help improve the interpretability of future neuroimaging studies, especially those in brain development, maturation and aging.

1. Introduction

Neurite orientation dispersion and density imaging (NODDI) is a popular compartment-based model in diffusion MRI for studying microstructural changes of brain tissue (Zhang et al., 2012). The model assumes that signals we measure originate from a combination of intra-neurite, extra-neurite and free water compartments, each of which

produces unique dependence of signal to diffusion-sensitising setting in a pulse sequence. This has allowed for compartment-specific measures of microstructural properties to be determined, such as intra-neurite fraction and orientation dispersion index. These NODDI-derived measures have been shown to reflect altered microstructural properties in various neurological and psychiatric disorders (Churchill et al., 2017; Fu et al., 2019; Kamagata et al., 2016; Rae et al., 2017; Sarrazin et al., 2019), as

Abbreviations: ACR, anterior corona radiata; ALIC, anterior limb of the internal capsule; BSS, body of corpus callosum; CSF, cerebrospinal fluid; EC, external capsule; GCC, genu of corpus callosum; GM, gray matter; IQR, interquartile range; NODDI, neurite orientation dispersion and density imaging; ODI, orientation dispersion index; PCR, posterior corona radiata; PLIC, posterior limb of the internal capsule; SCC, splenium of corpus callosum; SCR, superior corona radiata; SLF, superior longitudinal fasciculus; TE, echo time; WM, white matter.

* Corresponding author. Center for Brain Imaging Science and Technology, College of Biomedical Engineering and Instrumental Science, Zhejiang University, No. 38 Zheda Road, Hangzhou, 310027, China.

** Corresponding author. Center for Brain Imaging Science and Technology, College of Biomedical Engineering and Instrumental Science, Zhejiang University, No. 38 Zheda Road, Hangzhou, 310027, China.

E-mail addresses: hhezju@zju.edu.cn (H. He), jzhong@zju.edu.cn (J. Zhong).

<https://doi.org/10.1016/j.neuroimage.2020.116906>

Received 23 January 2020; Received in revised form 1 May 2020; Accepted 3 May 2020

Available online 7 May 2020

1053-8119/© 2020 The Author(s). Published by Elsevier Inc. This is an open access article under the CC BY-NC-ND license (<http://creativecommons.org/licenses/by-nc-nd/4.0/>).

well as in brain development, maturation and aging, across the whole lifespan, from the neonatal (Kansagra et al., 2016; Kunz et al., 2014) to adolescent (Geeraert et al., 2019; Mah et al., 2017) and adult period (Billiet et al., 2015; Chang et al., 2015; Cox et al., 2016; Kodiweera et al., 2016; Merluzzi et al., 2016; Nazeri et al., 2015). In addition, NODDI-derived intra-neurite fraction in combination with myelin-sensitive technique can provide estimation of the g-ratio (Jung et al., 2018; Stikov et al., 2015), which has been used as a marker of brain myelination during development (Dean et al., 2016).

Despite the popularity of NODDI for tracking brain changes throughout the lifespan, the intrinsic dependence of the derived diffusion parameters on T2 makes it suboptimal, especially for investigating brain development and maturation during which substantial alterations of T2 relaxation times have been well documented (Ding et al., 2004; Lee et al., 2018). Like the other contemporary compartment models in diffusion MRI (Alexander et al., 2010; Assaf and Basser, 2005; Jespersen et al., 2007; Novikov et al., 2018), the NODDI model does not explicitly consider the difference of T2 relaxation between compartments and the data is routinely acquired with a single echo time (TE). As a result, measures derived from those models, such as the signal fraction of each compartment, can be relaxation weighted (Lampinen et al., 2019). Thus, when differences of compartmental T2 exist, one cannot disentangle differences in diffusion from relaxation between compartments. For example, the much longer T2 in cerebrospinal fluid (CSF) compared to tissue has been shown to cause an overestimation of free water fraction in white matter (WM) with CSF contamination (Bouyagoub et al., 2016). Between the intra- and extra-neurite compartments, the difference of T2 (Peled et al., 1999; Wachowicz and Snyder, 2002), while much smaller in comparison, is known to cause TE-dependence of model-derived diffusion parameters in WM (De Santis et al., 2016b; Qin et al., 2009). This will be likely to have similar impact on NODDI-derived measures, potentially reducing the interpretability of the NODDI findings from studies where T2 changes dramatically, such as in brain development. There is a clear need to develop techniques that can disentangle non-T2-weighted NODDI measures from T2 relaxation.

One powerful approach to achieve this is to exploit the synergy between diffusion and T2 relaxation. The strategy was adopted in a seminal NMR study (Peled et al., 1999) to assign different T2 components in frog sciatic nerve to distinct tissue compartments, providing one of the first evidence for intra-axonal T2 being larger than extra-axonal T2. This relaxation-diffusion correlation technique was later extended to imaging (Benjamini and Basser, 2016; Kim et al., 2017), enabling applications in animal spinal cord (Benjamini and Basser, 2017; Kim et al., 2017) and in *ex vivo* human brain (Pas et al., 2020). More recently, this approach was combined with biophysical modelling to improve the estimation of tissue microstructure parameters for *in vivo* human brain imaging. For example, it has been demonstrated that combined modelling of diffusion and T2 relaxation, together with data acquired at multiple TEs, enables the distinction of compartment-specific T2 relaxation in WM and the estimation of non-T2-weighted diffusion parameters (Veraart et al., 2018). The combined modelling is later demonstrated with multi-dimensional b-tensor encoding (Lampinen et al., 2019).

Inspired by these studies, we propose to leverage the same strategy to estimate non-T2-weighted NODDI measures from diffusion data with multiple TEs; the resulting technique will be henceforth referred to as multi-TE NODDI (MTE-NODDI). The technique works by incorporating compartment-specific T2 relaxation times into the modelling of T2-weighted compartment fractions, thereby enabling non-T2-weighted fractions, together with compartment-specific T2 relaxation times, to be estimated directly from T2-weighted fractions. We demonstrate the TE-dependence of T2-weighted NODDI measures and assess the performance of MTE-NODDI for estimating their non-T2-weighted counterparts, as well as compartment-specific T2 values, with both simulation and *in vivo* human brain data acquired for multiple TEs, with a fixed diffusion time across TEs and b-values.

2. Theory

This section describes the theory behind the proposed technique to determine non-T2-weighted signal fractions in NODDI. A definition of the NODDI model is first provided that makes the TE-dependence of its T2-weighted signal fractions explicit. We then derive the analytical relationship between these T2-weighted signal fractions and their non-T2-weighted counterparts, which underpins the proposed MTE-NODDI technique. Finally, we show how the compartment-specific T2 relaxation times can be estimated at the same time.

2.1. NODDI and its T2-weighted signal fractions

NODDI is a multi-compartment model of diffusion for characterizing neuronal tissue. The model assumes the signal from any imaging voxel originate from two non-exchanging sources: the tissue and free water compartments. NODDI further models the signal from the tissue compartment as from two non-exchanging components: the intra-neurite and extra-neurite compartments.

The model can be expressed mathematically as:

$$A = (1 - f_{iso})(f_{in}A_{in} + (1 - f_{in})A_{en}) + f_{iso}A_{iso} \quad [1]$$

where A is the overall normalized diffusion-weighted signal; A_{in} , A_{en} and A_{iso} are the normalized signals of intra-neurite, extra-neurite and free water compartments; A_{in} is modelled as orientation-dispersed sticks with a Watson distribution (Zhang et al., 2011) or a Bingham distribution (Tariq et al., 2016), from which the orientation dispersion index (ODI) can be derived; A_{en} and A_{iso} are modelled as anisotropic and isotropic Gaussian diffusion respectively; f_{iso} is the signal fraction of the free water compartment, defined with respect to the overall signal such that $1 - f_{iso}$ corresponds to the signal fraction of the tissue compartment; f_{in} is the signal fraction of the intra-neurite compartment, defined with respect to the signal of the tissue compartment, such that $1 - f_{in}$ corresponds to the signal fraction of the extra-neurite compartment.

The signal fractions of f_{in} with respect to the signal of tissue, and f_{iso} with respect to overall signal can be expressed mathematically as:

$$f_{in} = \frac{S_{in}^0 e^{-TE/T_2^{in}}}{S_{in}^0 e^{-TE/T_2^{in}} + S_{en}^0 e^{-TE/T_2^{en}}} \quad [2]$$

$$f_{iso} = \frac{S_{iso}^0 e^{-TE/T_2^{iso}}}{S_{in}^0 e^{-TE/T_2^{in}} + S_{en}^0 e^{-TE/T_2^{en}} + S_{iso}^0 e^{-TE/T_2^{iso}}} \quad [3]$$

where S_{in}^0 , S_{en}^0 and S_{iso}^0 represent compartmental signals at $b = 0$ and $TE = 0$, and T_2^{in} , T_2^{en} and T_2^{iso} are T2 relaxation times for the intra-neurite, extra-neurite and free water compartments respectively. Since T2 of each compartment is different in general, both signal fractions are T2-weighted and will typically be TE dependent. In contrast, ODI, by definition, does not involve any signal fractions and thus should not exhibit TE dependence. With MTE data, we estimate its value as the arithmetic mean of the ODI's estimated for each TE. We explain in the following how the TE-dependence of signal fractions can be directly used to estimate their non-T2-weighted versions.

2.2. Estimation of non-T2-weighted signal fractions

We show here that the non-T2-weighted signal fractions can be directly related to the T2-weighted NODDI measures. First, we define the non-T2-weighted intra-neurite signal fraction with respect to the signal of tissue as $f_{in}^0 = \frac{S_{in}^0}{S_{in}^0 + S_{en}^0}$ and free water fraction with respect to the overall signal as $f_{iso}^0 = \frac{S_{iso}^0}{S_{in}^0 + S_{en}^0 + S_{iso}^0}$ respectively. Then we can rewrite the T2-weighted signal fractions in Eq. [2] and Eq. [3] in terms of f_{in}^0 and f_{iso}^0 as:

$$f_{in}(TE) = \frac{f_{in}^0 e^{-TE/T_2^{in}}}{f_{in}^0 e^{-TE/T_2^{in}} + (1 - f_{in}^0) e^{-TE/T_2^{en}}} \quad [4]$$

$$f_{iso}(TE) = \frac{f_{iso}^0 e^{-TE/T_2^{iso}}}{f_{iso}^0 e^{-TE/T_2^{iso}} + (1 - f_{iso}^0) [f_{in}^0 e^{-TE/T_2^{in}} + (1 - f_{in}^0) e^{-TE/T_2^{en}}]} \quad [5]$$

$$= \frac{f_{iso}^0 e^{-TE/T_2^{iso}}}{f_{iso}^0 e^{-TE/T_2^{iso}} + (1 - f_{iso}^0) f_{in}^0 e^{-TE/T_2^{in}} / f_{in}(TE)}$$

Eq. [4] shows that the NODDI-derived T2-weighted intra-neurite signal fraction is determined by its non-T2-weighted counterpart together with compartment-specific T2 values. In contrast, Eq. [5] shows that f_{in} also contributes to the TE-dependence of f_{iso} ; hence, estimating f_{in}^0 is prerequisite to determining f_{iso}^0 .

Eq. [4] also shows that it is only the difference of $1/T_2^{in}$ and $1/T_2^{en}$, not their respective values, dictates the TE-dependence of $f_{in}(TE)$, as it can be simplified further to:

$$f_{in}(TE) = \frac{f_{in}^0 e^{TE\Delta R_2^{en-in}}}{f_{in}^0 e^{TE\Delta R_2^{en-in}} + (1 - f_{in}^0)} \quad [6]$$

where $\Delta R_2^{en-in} = 1/T_2^{en} - 1/T_2^{in}$. This enables the estimation of f_{in}^0 and ΔR_2^{en-in} from $f_{in}(TE)$ for multiple TEs.

Similarly, Eq. [5] can be simplified to:

$$f_{iso}(TE) = \frac{f_{iso}^0 e^{TE\Delta R_2^{in-iso}}}{f_{iso}^0 e^{TE\Delta R_2^{in-iso}} + (1 - f_{iso}^0) f_{in}^0 / f_{in}(TE)} \quad [7]$$

where $\Delta R_2^{in-iso} = 1/T_2^{in} - 1/T_2^{iso}$. This enables the estimation of f_{iso}^0 and ΔR_2^{in-iso} , from $f_{iso}(TE)$ and $f_{in}(TE)$, as well as f_{in}^0 estimated from Eq. [6] above.

Finally, observe that Eq. [6] and Eq. [7] can be rewritten in the form of linear models, such that:

$$\ln \frac{f_{in}(TE)}{1 - f_{in}(TE)} = TE\Delta R_2^{en-in} + \ln \frac{f_{in}^0}{1 - f_{in}^0} \quad [8]$$

$$\ln \frac{f_{in}^0 f_{iso}(TE)}{f_{in}(TE)(1 - f_{iso}(TE))} = TE\Delta R_2^{in-iso} + \ln \frac{f_{iso}^0}{1 - f_{iso}^0}. \quad [9]$$

Eq. [8] suggests ΔR_2^{en-in} and f_{in}^0 can be immediately computed from the slope and the intercept respectively, following a simple linear least squares fitting. Furthermore, it shows that they can be estimated with data from two or more different TEs. Eq. [9] suggests the same is true for ΔR_2^{in-iso} and f_{iso}^0 . Moreover, they suggest if ΔR_2^{en-in} and ΔR_2^{in-iso} are positive, $f_{in}(TE)$ and $f_{iso}(TE)$ will increase when TE increases.

2.3. Estimation of compartment-specific T2 relaxation times

The compartment-specific T2 relaxation times can be subsequently estimated from $b = 0$ signals acquired at multiple TEs. We first express the overall $b = 0$ signal as the sum of the $b = 0$ signals from the compartments, such that

$$S(b=0, TE) = S_{in}^0 e^{-TE/T_2^{in}} + S_{en}^0 e^{-TE/T_2^{en}} + S_{iso}^0 e^{-TE/T_2^{iso}}. \quad [10]$$

Substituting $f_{in}(TE)$ from Eq. [2] and $f_{iso}(TE)$ from Eq. [3], we have

$$S(b=0, TE) f_{in}(TE) (1 - f_{iso}(TE)) = S_{in}^0 e^{-TE/T_2^{in}} \quad [11]$$

which can be rewritten in the form of a linear model as

$$\ln[S(b=0, TE) f_{in}(TE) (1 - f_{iso}(TE))] = -\frac{TE}{T_2^{in}} + \ln S_{in}^0. \quad [12]$$

Hence, T_2^{in} can similarly be estimated from $f_{in}(TE)$ and $f_{iso}(TE)$ at

multiple TEs. And T_2^{en} and T_2^{iso} can be subsequently calculated from ΔR_2^{en-in} and ΔR_2^{in-iso} determined previously. Since the TE range typically used in diffusion studies is not sensitive to the long T_2^{iso} , we focus mainly on T_2^{in} and T_2^{en} within tissue compartments.

3. Materials and methods

This section describes the datasets, implementation and experiments used to assess the MTE-NODDI technique. Both the acquisition of the *in vivo* imaging data and the synthesis of simulated data were given in details, followed by the implementation details and experiments conducted.

3.1. Datasets

3.1.1. In vivo data

To explore TE-dependence of NODDI-derived parameters and assess the proposed technique, two healthy subjects (#1: male, 24-year-old; #2: female, 25-year-old) underwent diffusion-weighted imaging on a Siemens 3T Prisma scanner (Siemens, Erlangen, Germany) with a 64-channel head-neck coil. The local ethical committee approved this study and a written informed consent was obtained from each participant.

To exclude possible dependence on diffusion time (Fieremans et al., 2016), a prototype diffusion sequence allowing fixed diffusion time was employed. The otherwise identical protocol was repeated with 7 TE at 68, 78, 88, 98, 108, 118 and 132 ms respectively. The protocol details are as follows: three $b = 0$ s/mm² images, and monopolar diffusion weightings of $b = 1000, 2000$ and 3000 s/mm² applied along 30 isotropically distributed directions; three $b = 0$ s/mm² images in the reversed phase-encoding direction; diffusion times were fixed, with gradient width and separation $\delta/\Delta = 17.1/32.5$ ms for all b-values and TE's. Other imaging parameters: TR = 4000 ms; FOV = 225 × 225 mm²; slice number = 50; resolution = 2.5 × 2.5 × 2.5 mm³; slice acceleration factor = 2; phase acceleration factor = 2; bandwidth = 2416 Hz/pixel. Total imaging time was 50 min.

3.1.2. Simulations

To assess the accuracy and precision of the proposed technique with known ground truth, data from three typical WM voxels (without, affected and dominated by CSF contamination) were simulated with the NODDI MATLAB toolbox, modified to incorporate TE dependence. The acquisition protocol of simulated data was identical to the *in vivo* data protocol. The underlying parameter values of WM configuration were chosen in accordance with *in vivo* measurement from a typical voxel at internal capsule, and were as follows: $f_{in}^0 = 0.5$, $T_2^{in} = 90$ ms, $T_2^{en} = 60$ ms; concentration and mean orientation of Watson distribution: kappa = 2.5 (corresponding to ODI = 0.24), theta = 1, phi = 2; intrinsic free diffusivity and isotropic diffusivity: $D_1 = 1.7 \times 10^{-3}$ mm² s⁻¹ and $D_{iso} = 3 \times 10^{-3}$ mm² s⁻¹ respectively (Alexander et al., 2010; Zhang et al., 2011); $T_2^{iso} = 1000$ ms and $f_{iso}^0 = 0/0.1/0.5$ respectively for the three voxels without, affected and dominated by CSF contamination. Each voxel was simulated for 1000 random Rician noise realizations in the magnitude signal by $S_{noise} = \sqrt{(S + \sigma)^2 + \sigma^2}$, in which the standard deviation of Gaussian noise level σ was fixed for all signals achieving a SNR of $S(b = 0, TE = 98 \text{ ms})/\sigma = 50$ for pure WM voxel seen *in vivo*.

More extensive simulation experiments were performed with a variety of different scenarios, including: (1) different T_2^{in} and T_2^{en} values; (2) different SNRs; (3) different intrinsic free diffusivities. The details can be found in [supplementary material S.1-S.3](#).

3.2. Implementation and experiments

3.2.1. Pre-processing and NODDI estimations

To reduce the effect of noise and imaging artifacts for the *in vivo*

diffusion data, signal noise was first reduced by applying a method based on random matrix theory (Veraart et al., 2016) separately for each TE session, followed by the correction of B0 inhomogeneity, eddy current and motion with TOPUP (Andersson and Sotiropoulos, 2016) and EDDY (Andersson et al., 2016) in FMRIB Software Library (FSL, University of Oxford, UK). NODDI-derived parameters were estimated for each TE session with the NODDI MATLAB Toolbox, and the estimated parameters were rigidly aligned to the first TE session. For the simulation data, NODDI-derived measures were directly estimated with no pre-processing steps.

3.2.2. Demonstration of TE-dependence of NODDI estimations

To demonstrate the TE dependence of NODDI-derived parameters for *in vivo* data, ROI-based analysis as a function of TE was conducted. Anatomical ROIs were extracted from the Johns Hopkins University (JHU) WM atlas (Mori et al., 2005) by the following process: the T2-weighted $b = 0$ image was registered to the standard T2-weighted image in JHU space using non-linear registration with FNIRT in FSL (Smith et al., 2004); The inverse of the resulting warp field was applied to the WM atlas to transform the ROIs into the subject space. The ROIs studied were chosen in accordance with previous studies (McKinnon and Jensen, 2019; Veraart et al., 2018): the genu (GCC), splenium (SCC), and body (BCC) of the corpus callosum, the anterior (ACR), superior (SCR), and posterior (PCR) corona radiata, the anterior and posterior limb of the internal capsule (ALIC and PLIC, respectively), the external capsule (EC), and the superior longitudinal fasciculus (SLF) (combined from both hemispheres). To illustrate TE-dependence in gray matter (GM), the frontal pole ROI was extracted from the Harvard-Oxford cortical atlas (Desikan et al., 2006).

3.2.3. Compartment-specific non-T2-weighted fractions and T2 estimations

After demonstrating TE-dependence, the MTE-NODDI was implemented for simulation data to assess the accuracy and precision of estimations, and for *in vivo* data, with the following implementation details.

Following the theory section, the T2-independent f_{in}^0 and ΔR_2^{en-in} were first estimated from Eq. [6] using the NODDI estimates from data of the 7 TEs with non-linear least squares estimation. Each fit was initialized using one random starting point sampled from following parameter ranges: $0 \leq f_{in}^0 \leq 1$, $-0.03 \leq \Delta R_2^{en-in} \leq 0.03 \text{ms}^{-1}$ (determined by assuming $28 \leq T_2^{en}, T_2^{in} \leq 200 \text{ms}$). The resulting estimates were used to determine f_{iso}^0 from Eq. [7]. Initialization values for each fit were generated randomly from following parameter ranges: $0 \leq f_{iso}^0 \leq 1$, $0.004 \leq \Delta R_2^{in-iso} \leq 0.024 \text{ms}^{-1}$ (determined by assuming $40 \leq T_2^{in} \leq 200 \text{ms}$; $T_2^{iso} = 1000 \text{ms}$). The T2 ranges are in accordance with or wider than the ranges of these parameters found in the literature (MacKay et al., 2006; MacKay and Laule, 2016). The termination tolerance of all fittings on residual sum of squares and changes between iterations are 10^{-10} with a maximum iteration of 1000 times. The optimization algorithm chosen for non-linear least squares uses an interior trust region approach (Coleman and Li, 1996); lower and upper bounds for the parameters were set to their respective initialization range. T_2^{in} was estimated using Eq. [12] from the NODDI estimates and $b = 0$ measurements of the 7 TEs with linear least squares, and T_2^{en} was calculated using the estimated T_2^{in} and ΔR_2^{en-in} .

3.2.4. Robustness of MTE-NODDI to the number of TEs

To assess the robustness of the MTE-NODDI, we evaluated the estimation performance when the number of TE measurements were progressively reduced. For any given number of TEs, we considered two scenarios: 1) keeping the same minimum and maximum TEs of the full set to maximise the TE range; 2) keeping only the shortest TEs to maximise SNR. The cases maximising the TE range are: 2 TEs (68, 132 ms), 3 TEs (68, 98, 132 ms) and 4 TEs (68, 88, 108, 132 ms); The cases maximising SNR are: 3 TEs (68, 78, 88 ms), 4 TEs (68, 78, 88, 98 ms) and 5 TEs (68, 78, 88, 98, 108 ms). Experiments were conducted on *in vivo* data, and on

simulation data corresponding to the pure WM voxel. The estimation process and the optimization settings were the same as described above.

4. Results

4.1. TE-dependence of NODDI-derived parameters in *in vivo* data

Fig. 1 shows the NODDI-derived f_{in} , ODI and f_{iso} maps from Subject #1 at each TE, while Fig. 2 plots the mean and standard deviation of these parameters for the set of chosen WM and GM ROIs as a function of TE. As demonstrated qualitatively in Fig. 1 and quantitatively in Fig. 2, f_{in} increases with TE in all WM ROIs but remains relatively constant in the GM ROI, suggesting ΔR_2^{en-in} is positive in WM but is negligible in GM. f_{iso} increases in both WM and GM ROIs, as expected, given the positive ΔR_2^{in-iso} , a result of T_2^{iso} being much longer than T_2^{in} . The standard deviations of these two parameters also slightly increase when TE increases, possibly a result of both decreased SNR and regional variation of ΔR_2^{en-in} and ΔR_2^{in-iso} . In contrast, ODI shows minimal TE-dependence, as expected.

4.2. Simulations: accuracy and precision of NODDI and MTE-NODDI estimates

The distributions of all estimates of the 1000 Rician noise realization for three WM voxels are shown as boxplots in Fig. 3. The NODDI estimates of signal fractions from the simulation data demonstrate the same TE-dependence as *in vivo* data, with the slope of increasing $f_{in}(TE)$ determined by the T2 difference of intra-neurite and extra-neurite compartments, i.e. the ΔR_2^{en-in} , as demonstrated in supplementary material S.1. Similarly, the ODI shows little TE-dependence as *in vivo* data. Unsurprisingly, the ODI for the MTE-NODDI data as a whole demonstrates considerably higher precision than the corresponding values for each individual TE.

Focusing on the new parameters provided by MTE-NODDI, the mean and standard deviation of their estimated values are given in Table 1. The MTE-NODDI estimates overall show high accuracy and precision compared to the ground truth. For the pure WM voxel, there is a slight negative bias to the f_{in}^0 and T_2^{en} , and a slight positive bias to T_2^{in} . This is introduced by the Rician noise, which causes a positive bias to NODDI-derived T2-weighted fractions, especially for higher TE with lower SNR. As demonstrated in supplementary material S.2, higher SNR reduces the bias, while lower SNR increases it. The precision of estimated parameters was reflected by the interquartile range (IQR) in Fig. 2 and the standard deviation in Table 1. The IQR increases from 0.011 to 0.029 for T2-weighted f_{in} from TE = 68 to TE = 132 ms, and the IQR for modelled f_{in}^0 is 0.039, indicating the noise is slightly amplified in the estimation of f_{in}^0 . The IQR for T_2^{in} and T_2^{en} are 2.268 and 4.941 ms respectively, suggesting a higher precision of T_2^{in} than T_2^{en} .

For voxels with CSF contamination, it is interesting to note that the T_2^{in} is not heavily affected because the consideration of the free water compartment. The effective SNR for WM signal is lower, reflected by the wider IQR of estimated f_{in} than pure WM voxel. However, the SNR for the total signal is higher, hence reducing the estimation bias caused by Rician noise to some extent considering the two factors. Overall, the simulation results suggest a high accuracy and precision of f_{in}^0 , f_{iso}^0 and T_2^{in} estimation, and that the precision of T_2^{en} , which is determined by previously estimated ΔR_2^{en-in} and T_2^{in} , is less robust than T_2^{in} estimation, especially when CSF contamination exists.

4.3. *In vivo* data: TE-independent parameter estimates

The estimated maps of T2-independent parameters from both subjects are shown together with their whole-brain WM histograms in Fig. 4. Again, we focus on the new parameters provided by MTE-NODDI; the

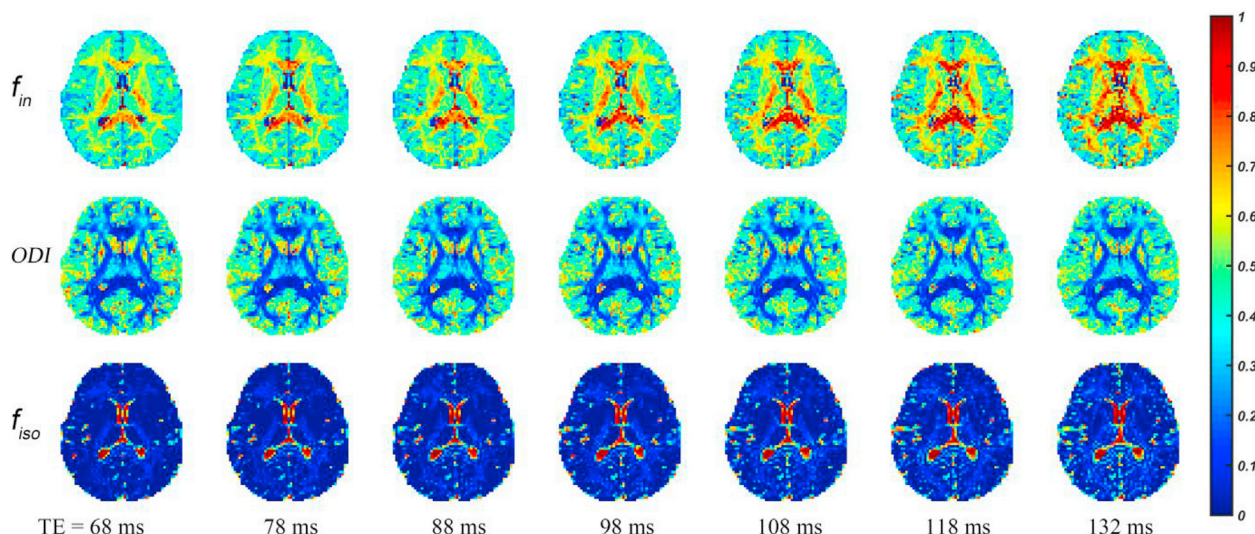


Fig. 1. Conventional NODDI-derived f_{in} , ODI, and f_{iso} maps at different TEs from subject #1. As TE increases, there are visually appreciable increases of f_{in} and f_{iso} in WM.

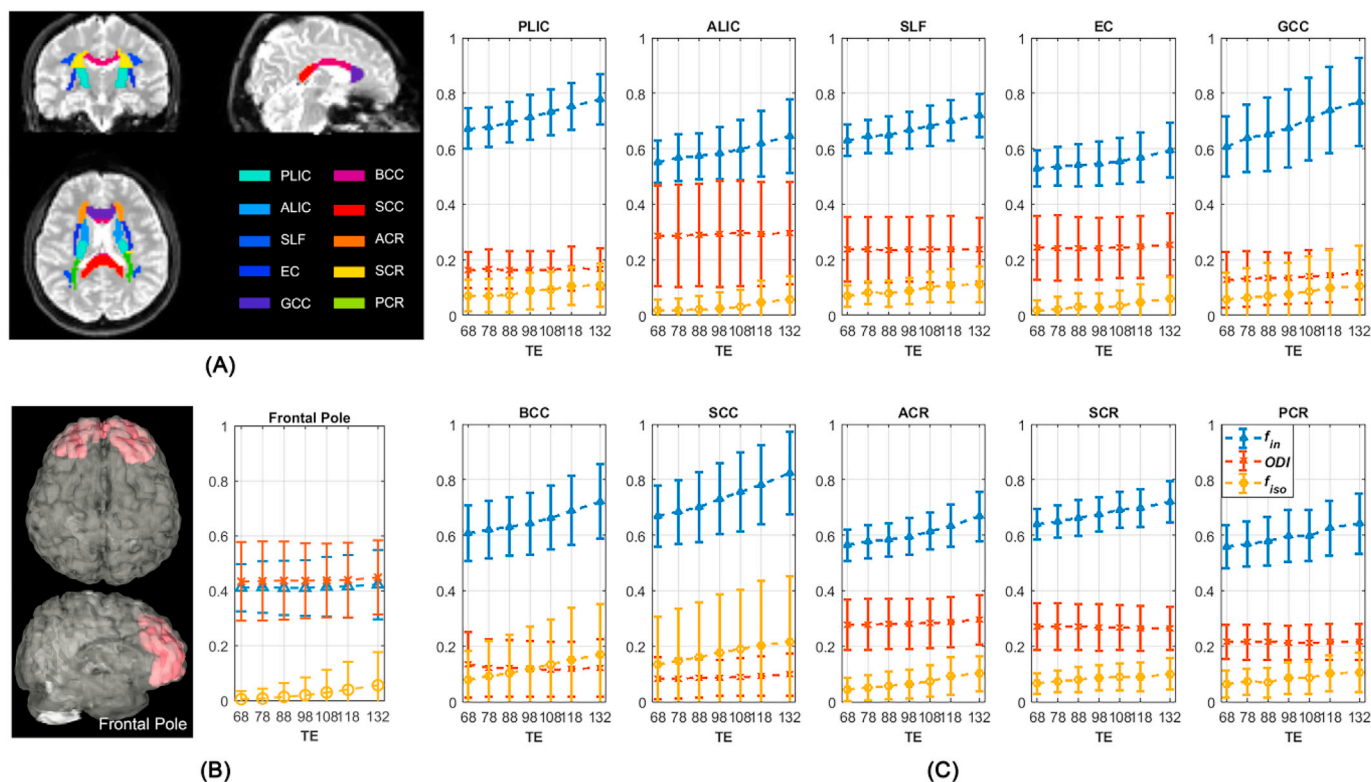


Fig. 2. Demonstration of TE-dependence of NODDI-derived f_{in} , ODI, and f_{iso} in the set of chosen WM (A)(C) and GM (B) ROIs from subject #1. The mean and standard deviation of the parameters within the ROIs are plotted against TE. f_{in} shows increasing trend in all WM ROIs while remains relatively constant in the GM ROI; f_{iso} shows increasing trend in all ROIs; and ODI remains relatively constant in all ROIs.

ODI maps are included in [supplementary material S.4](#). The following observations can be made: First, the conventional NODDI-derived T2-weighted intra-neurite and CSF fractions shown in Fig. 2 are over-estimated with respect to their non-T2-weighted counterparts. The mean of the non-T2-weighted f_{in}^0 in WM is about 0.46, while its T2-weighted version ranges from 0.60 at TE = 68 ms to 0.71 at TE = 132 ms; the mean of the non-T2-weighted f_{iso}^0 in WM is about 0.04, while its T2-weighted version ranges from 0.07 at TE = 68 ms to 0.13 at TE = 132 ms. Second, the estimated ΔR_2^{in} in WM is consistently positive,

indicating $T_2^{in} > T_2^{en}$ in WM. Third, the parameter estimates for MTE-NODDI show high consistency between the two subjects, as reflected by the overlapping parameter histograms. The mean and standard deviation of f_{in}^0 are 0.46 ± 0.14 for Subject #1 and 0.46 ± 0.13 for Subjects #2; for f_{iso}^0 , they are 0.03 ± 0.05 and 0.04 ± 0.06 ; for compartment T2, they are 82 ± 18 ms and 83 ± 17 ms for T_2^{in} and 51 ± 17 ms and 53 ± 17 ms for T_2^{en} respectively.

The detailed WM ROI-based analysis of these parameters are shown in Fig. 5. The variations of the estimated parameters across different ROIs

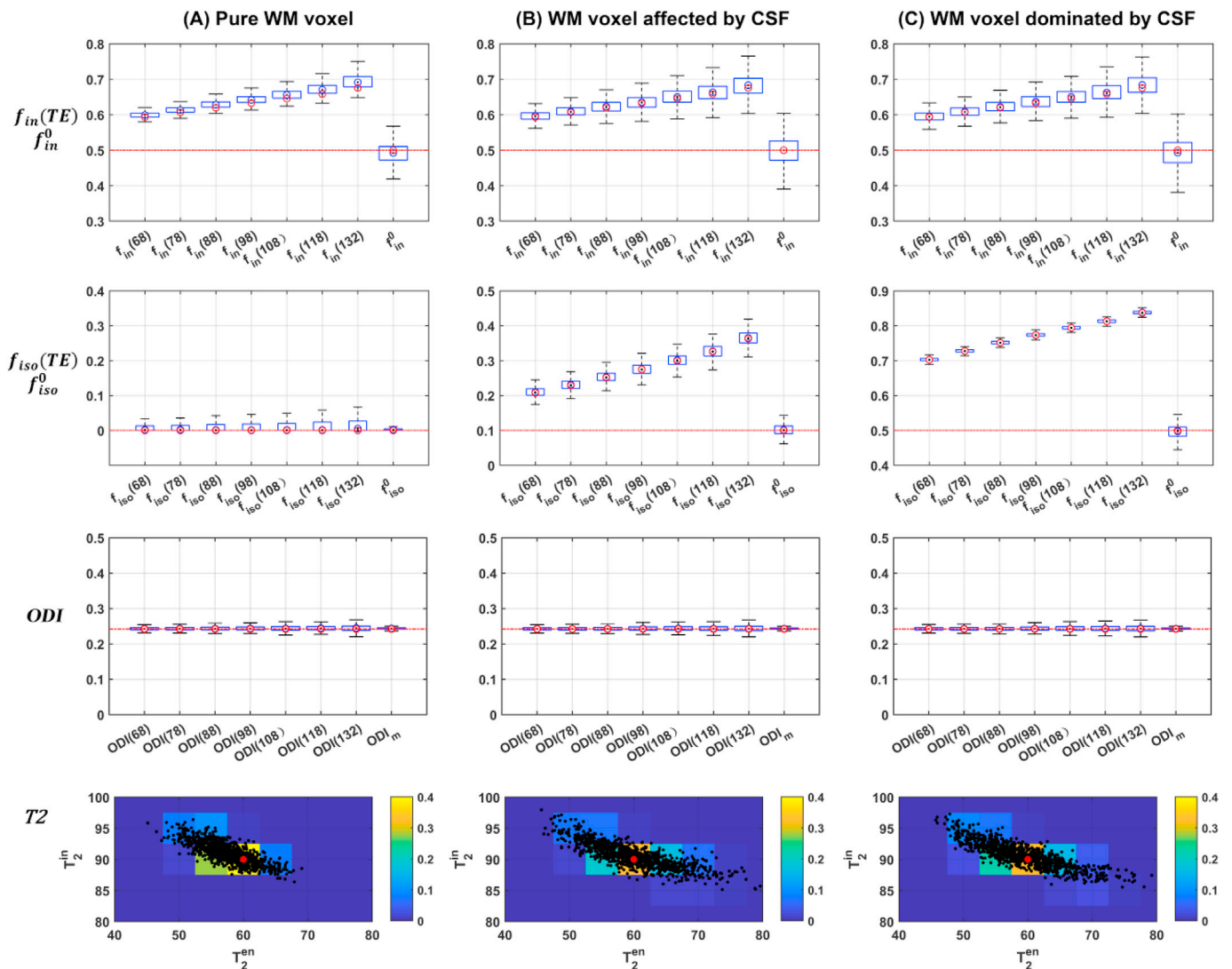


Fig. 3. Distributions of all estimates from simulation data for (a) pure WM voxel ($f_{iso}^0=0$); (b) WM voxel affected by CSF ($f_{iso}^0=0.1$); (c) WM voxel dominated by CSF ($f_{iso}^0=0.5$). In the boxplots, the TE-dependence of NODDI-derived T2 weighted fractions display the same tendency as *in vivo* data, and the following MTE-NODDI derived non-T2-weighted counterparts display minimal bias; the ODI's estimated from individual TE display little TE-dependence as *in vivo* data, and the following ODI's for MTE-NODDI data display higher precision; the blue box and blue dot reflect the interquartile range (IQR) and the median of 1000 Rician noise estimations respectively and the red dot reflects the estimation without noise. The distributions of estimated T_2^m (ms) and T_2^e (ms) are displayed as black dots with their probabilities indicated by colour.

Table 1

Mean/standard deviation of MTE-NODDI estimates from three WM configurations (a-c) with their ground truth given at first row.

$f_{in}^0=0.5$; $T_2^m = 90$ ms; $T_2^e = 60$ ms	(a) $f_{iso}^0 = 0$	(b) $f_{iso}^0 = 0.1$	(c) $f_{iso}^0 = 0.5$
f_{in}^0	0.491/0.029	0.498// 0.041	0.493/0.042
f_{iso}^0	0.003/0.003	0.103/0.016	0.497/0.020
T_2^m /ms	91.035/ 1.668	90.579/ 1.972	90.697/ 1.982
T_2^e /ms	57.564/ 3.744	59.884/ 5.948	59.160/ 5.851

are considerable, especially for compartmental T2 values. While the mean f_{in}^0 is from 0.40 to 0.54 and f_{iso}^0 is below 0.1, T_2^m varies from 69 ± 6 ms from EC to 94 ± 15 ms from PLIC; and T_2^e varies from 42 ± 17 ms from GCC 61 ± 12 ms from PCR. These regional variations are consistent between the subjects and in keeping with previous literature (McKinnon and

Jensen, 2019; Veraart et al., 2018). In comparison, for all the ROIs, between-subject differences are considerably smaller, demonstrating the robustness of the technique.

4.4. Robustness of MTE-NODDI estimates to the number of TEs

The results from simulation using the pure WM voxel are shown in Fig. 6. The estimates with full data of 7 TEs, shown previously in Fig. 2, are included for reference, which demonstrates slight biases relative to the ground truth. When reducing the number of TEs, at the same time keeping the shortest TEs, the strategy includes the least biased NODDI-derived TE-dependent fractions, which slightly reduces the biases of the MTE-NODDI parameters: reducing the underestimation of f_{in}^0 and T_2^m and the overestimation of T_2^e and ΔR_2^{e-in} . However, the estimation precision of f_{in}^0 , T_2^m and especially ΔR_2^{e-in} are noticeably reduced reflected by the wider IQR with 4 and 3 TEs; the precision of T_2^e is affected more as it is calculated from ΔR_2^{e-in} and T_2^m . In contrast, when reducing the number of TEs while keeping the same TE range, the accuracy and precision of parameter estimation closely mirror those of the full data,

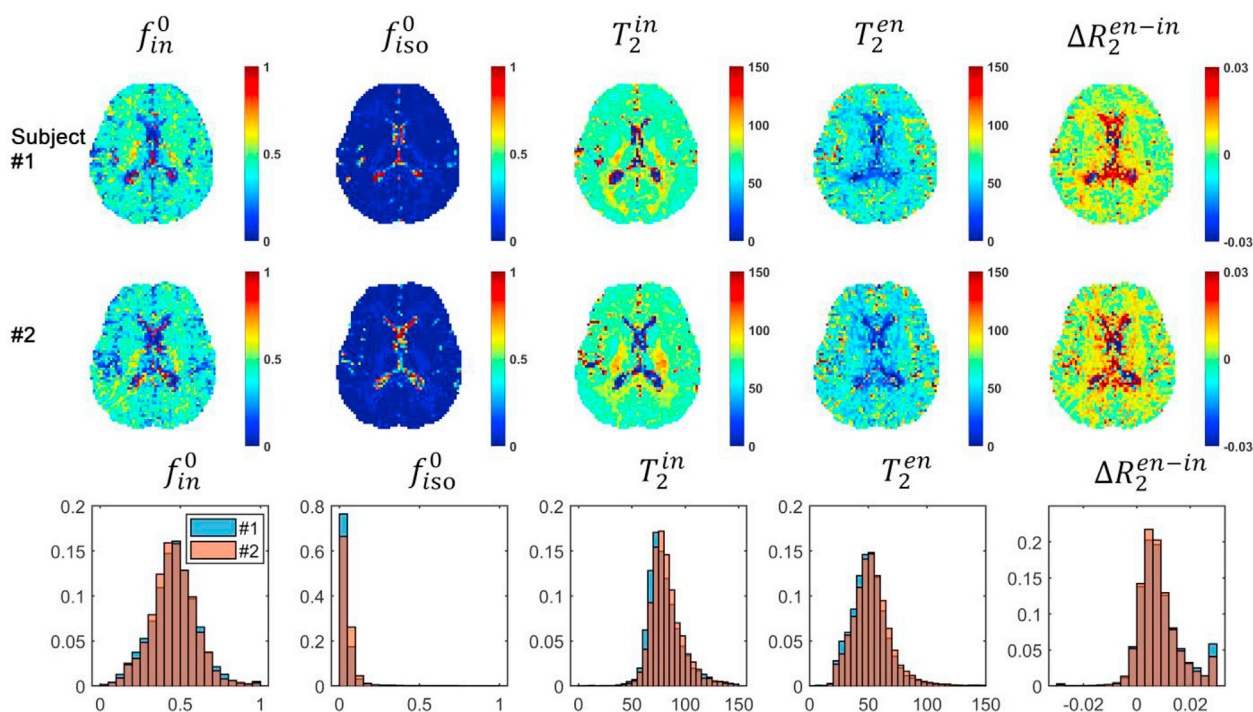


Fig. 4. MTE-NODDI estimated parameter maps and histograms of whole-brain WM voxels from both subjects. The parameter estimates show high consistency between the two subjects. In WM, f_{in}^0 is around 0.5, and $T_2^{in} > T_2^{en}$ (ms) generally.

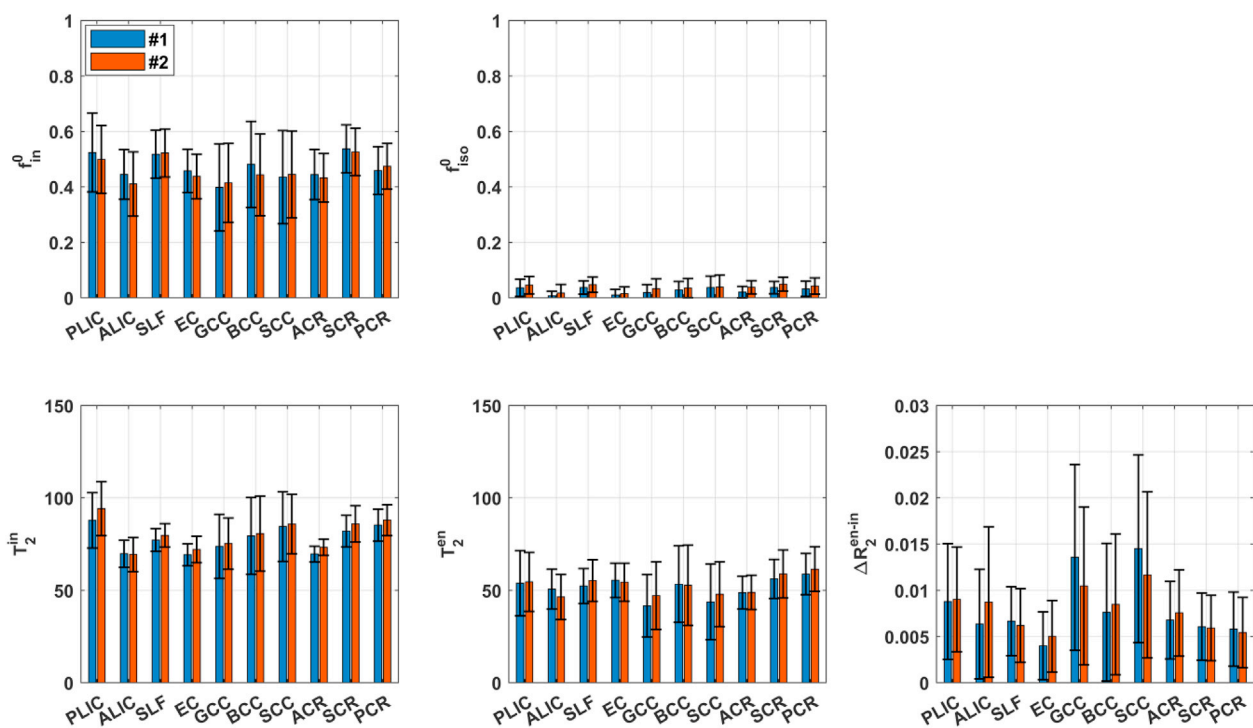


Fig. 5. The mean and standard deviation of the estimated parameters for the chosen WM ROIs for subject #1 and #2. There are considerable regional variations, which are consistent between subjects.

including the slight biases.

The results from *in vivo* data, shown in Fig. 7, are consistent with the results from simulation data. When keeping the same TE range, the estimated parameters are robust to reducing the number of TEs, especially for the signal fractions and T_2^{in} estimation, even with only 2 TEs, the minimum requirement. In contrast, when keeping the shortest TEs, there

is a slight increasing trend for f_{in}^0 and decreasing trend of T_2^{in} , corresponding to the simulation results. However, reducing the TE range reduces the precision of parameter estimation, especially for ΔR_2^{en-in} , which in turn affects the T_2^{en} estimation. One possible solution is to impose the constraint of $0 \leq \Delta R_2^{en-in} \leq 0.03$ during fitting, given that the full data has demonstrated $T_2^{en} \leq T_2^{in}$. By imposing this narrower range of ΔR_2^{en-in} ,

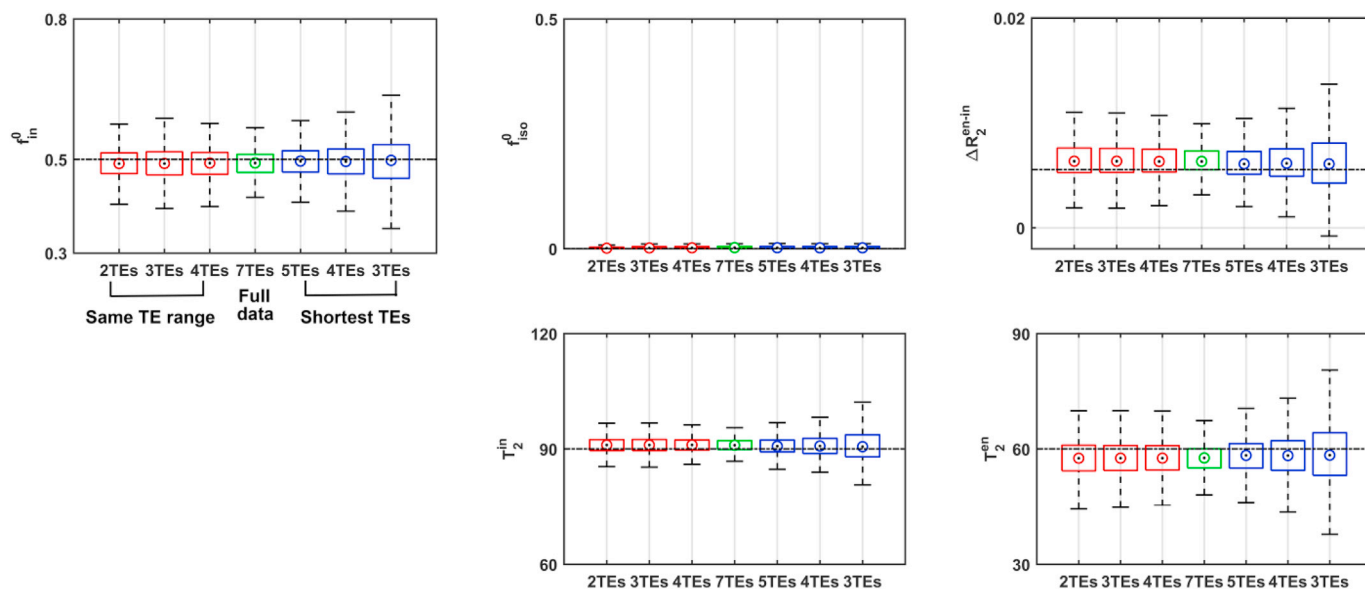


Fig. 6. The dependence of parameter estimates from simulation data of pure WM voxel on the number and range of TEs. Boxplots of 1000 noise realizations are shown for each case.

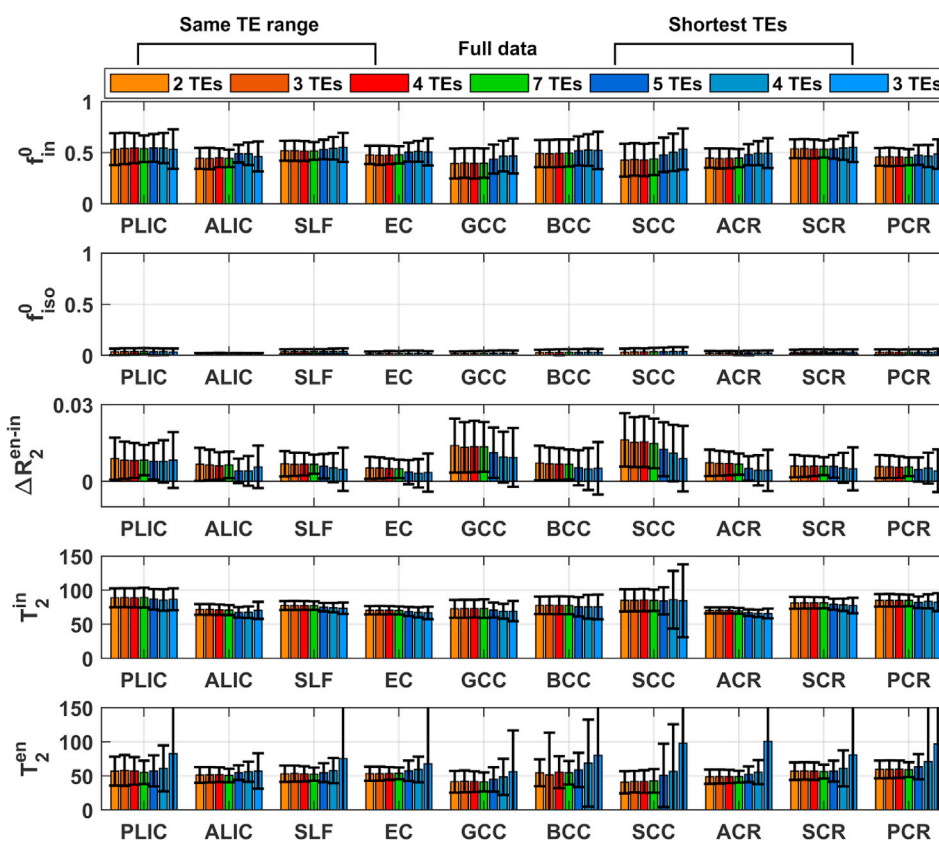


Fig. 7. The dependence of parameter estimates from *in vivo* data on the number and range of TEs. The mean and standard deviation of each parameter for all the WM ROIs are shown for each case.

the outlier estimates of T_2^{en} are noticeably reduced as demonstrated in [supplementary material S.5](#).

5. Discussion and conclusion

In summary, this study proposes MTE-NODDI technique to derive the non-T2-weighted compartment fractions and compartment-specific T2

relaxations, and demonstrates it with both *in vivo* and simulation data. The simulation data demonstrates the accuracy and precision of MTE-NODDI, and the *in vivo* data demonstrates the TE-dependence of NODDI estimated parameters and the ability of MTE-NODDI to exploit such TE-dependence. Compared to NODDI estimates, the estimates from MTE-NODDI suggest that conventional T2-weighted signal fractions will give overestimated relative intra-neurite and CSF fractions, due to the

estimated T_2^{in} being larger than T_2^{ex} from the proposed technique, and $T_2^{iso} \gg T_2^{in}$ in studies respectively. Meanwhile, the T2-weighted intra-neurite and CSF fractions will increase with TE. By disentangling the non-T2-weighted compartment fraction with its specific relaxation, the MTE-NODDI technique could facilitate the interpretation and quantification of studies where alteration of T2 and fraction interacts and where acquisition protocols (e.g. TE) are different.

The MTE-NODDI estimated non-T2-weighted intra-neurite fraction and intra- and extra-neurite T2 values for *in vivo* data correspond well with previous related studies. For the estimation of non-T2 weighted fractions, our results for f_{in}^0 in WM ROIs are largely consistent with those obtained from the TEDDI method (Veraart et al., 2018), though the TEDDI method differs from ours in being an integrated two-compartment model for WM voxels requiring complex fitting. For the estimation of compartment-specific T2 relaxations, our results are also largely consistent with both those obtained by TEDDI method (Veraart et al., 2018) and by the direction-averaged diffusion method (McKinnon and Jensen, 2019). We did additionally consider the CSF compartment, hence mitigated the problem of inaccurate T2 estimation with two-compartment model in areas with CSF contamination (Veraart et al., 2018). Actually, the rationale behind T_2^{in} estimations for our technique and (McKinnon and Jensen, 2019) is similar. However (McKinnon and Jensen, 2019), approximated the T2-weighted intra-neurite water fraction by using direction-averaged signals from high b-value up to 8000 s/mm², in which the signals from extra-neurite and CSF were suppressed. In contrast, we use NODDI model estimations of intra-neurite and CSF water fraction from comparatively lower b-values which is clinical feasible in most scanners. Meanwhile, compared to these two studies (McKinnon and Jensen, 2019; Veraart et al., 2018), the fixed diffusion time in our study eliminates the possibility of diffusion time dependence (Fieremans et al., 2016) as a confounding factor to the findings.

Exploiting the compartment-specific T2 values estimated from T2 relaxometry methods could be another way to calibrate the T2-weighted signal fractions from diffusion model, as demonstrated by (Bouyagoub et al., 2016) to correct for the overestimation of CSF-fraction. However, this method assumes a single T2 in tissue, hence could not provide non-T2-weighted estimates of intra-neurite fraction. While a study using multi-echo T2 relaxometry suggested the T2 values of the intra- and extra-neurite spaces of tissue could be different (Whittall et al., 1997), differentiating distinct T2 values with relaxometry methods alone was found challenging due to the limited SNR available (Graham et al., 1996). By combining relaxation and diffusion in a study of frog sciatic nerve, Peled et al. (1999) observed a component with intermediate T2 and unrestricted diffusion consistent with extra-axonal water, and a component with long T2 and restricted diffusion consistent with intra-axonal water. This seminal study has inspired many techniques to combine relaxation and diffusion. Recent examples include diffusion-relaxation correlation imaging techniques (Benjamini and Basser, 2017, 2016; Kim et al., 2017) which have been used to study *ex vivo* human brain (Pas et al., 2020). These diffusion-relaxation correlation methods estimate a 2D spectrum without assuming the number of compartments *a priori*. In contrast, our modelling-based method extract diffusion and T2 relaxation parameters from a pre-defined set of compartments, which help reducing the data requirement, hence, making the technique potentially more clinically feasible. Future work could also take T1 relaxation into consideration (De Santis et al., 2016a) to further improve the specificity of estimated parameters.

The underlying microanatomical mechanisms of the estimated T2 difference between T_2^{in} and T_2^{ex} remain unclear, but one contribution factor could be the water exchange between myelin and intra/extra-neurite compartments. One thing noted first, signal directly from myelin is not considered in our study as well as in most diffusion studies, because of the minimal TE (68 ms) being considerably longer than the T2 of myelin. However, as validated by (Lin et al., 2018) with Mote Carlo simulation in a tissue model, the water exchange between myelin and

intra/extra-neurite compartments can lead to difference of measured T2 ($T_2^{in} > T_2^{ex}$), which plays a similar role as the difference of intrinsic T2 in causing TE-dependence of diffusion tensor-derived measures. Since the water exchange between intra/extra-neurite space and myelin sheath is mediated by the surface-to-volume ratio of myelin water, therefore affected by g-ratio, the simulation study further showed that increased g-ratio during demyelination process can reduce the TE-dependence. This inspired two of our hypotheses: first, the varying g-ratio across regions (Campbell et al., 2018) could be a possible contribution of the measured regional variation of the difference of T_2^{in} and T_2^{ex} ; second, hence decreased T2 difference estimated from our technique could possibly indicate demyelination process. Proofs of these hypotheses need not only simulation validation but more importantly histology correspondence. Future work will put emphasis on the validation.

Sequence optimization to reduce acquisition time must balance the need to reduce noise and to increase the TE range. On the one hand, the Rician noise is known to cause a positive bias to MRI magnitude signals. As has been demonstrated in the original NODDI paper (Zhang et al., 2012) and further confirmed in our simulation results, the biased signals introduce a slight positive bias to NODDI-derived T2-weighted parameters, especially for data from longer TE, which in turn introduces slight biases to the MTE-NODDI parameters. This argues for the use of TEs that are as short as possible. On the other hand, the estimation of relaxation parameters can benefit from widening the TE range. Our *in vivo* data suggests, considering the precision alone, the positive effect from keeping the longest TE outweighs the negative effect from reducing the SNR. Future work will exploit sequence optimization algorithms, such as (Alexander, 2008) to identify and test the most economical acquisition protocol for specific applications.

As a technique based on NODDI estimations, the MTE-NODDI inherits the limitations of model assumptions from NODDI, including tortuosity assumption and fixed diffusivities. Despite these, NODDI metrics have been shown to correlate with their histological counterparts (Grussu et al., 2017). The fixed diffusivity used in NODDI by default has been shown to be appropriate for WM across lifespan except for infancy (Guerrero et al., 2019). Moreover, our simulation results (supplementary material S.3) suggest only slightly negative bias of T_2^{ex} when actual diffusivity is lower, and slightly decreased precision of T_2^{ex} when actual diffusivity is higher. In contrast, T_2^{in} estimation is not affected as much. The robust estimates from NODDI allow us to exploit its TE-dependence with MTE-NODDI technique, the estimation speed of which can be largely accelerated (Daducci et al., 2015). Compared with the alternative of incorporating all the MTE-NODDI parameters into a joint estimation process with multi-TE diffusion data, the separate modelling of MTE-NODDI might sacrifice the specificity of estimated measures during intermediate steps, however, also mitigate the problem of joint estimation with increased complexity of modelling and difficulty in fitting.

Another limitation of the current proof-of-concept is its long acquisition time. Our experiments with reduced numbers of TEs suggest the possibility to reduce scan time considerably. Moreover, we anticipate that even shorter acquisition may be possible from exploiting recent advances in deep-learning-based diffusion model reconstruction method that could provide accurate parameter estimation from sparse acquisition. For example, recent works have demonstrated over 10-fold reduction of diffusion data with deep learning method for conventional NODDI estimation (Gibbons et al., 2019; Golkov et al., 2016), as well as other complex tissue properties in diffusion MRI (Li et al., 2019; Lin et al., 2019). These approaches can be used to reduce the acquisition time for MTE-NODDI to under 5 min, the exploration of which represents an important avenue for future work.

For future applications, the MTE-NODDI could be beneficial to the understanding and interpretability of neuroimaging studies, especially for those investigating age-related brain alterations, in which substantial alterations of T2-weighted intra-neurite fraction and T2 relaxation time have been reported throughout the lifespan. For example, the T2-

weighted intra-neurite fractions have been shown to increase during brain development (Kansagra et al., 2016) and maturation (Geeraert et al., 2019; Mah et al., 2017), followed with a plateau at adulthood (Kodiweera et al., 2016) and to decrease during aging (Cox et al., 2016; Merluzzi et al., 2016). In contrast, the T2 values in WM have been shown to decrease quickly during early development and decrease slower during maturation (Ding et al., 2004; Lee et al., 2018), followed by increasing in most brain regions and declining in a few regions during aging (Kumar et al., 2012). However, the intrinsic microstructural changes behind the development process remain unclear due to the limitations of conventional single TE method. With the ability to disentangle the T2-weighted signal fraction from T2 weighting, the MTE-NODDI developed in this study can be applied.

CRedit authorship contribution statement

Ting Gong: Conceptualization, Methodology, Software, Formal analysis, Validation, Investigation, Writing - original draft, Writing - review & editing, Visualization. **Qiqi Tong:** Investigation. **Hongjian He:** Resources, Writing - review & editing, Funding acquisition, Supervision. **Yi Sun:** Resources. **Jianhui Zhong:** Conceptualization, Resources, Writing - review & editing, Supervision. **Hui Zhang:** Conceptualization, Methodology, Resources, Writing - review & editing, Supervision.

Acknowledgement

This work was supported by the National Natural Science Foundation of China (81871428); the Shanghai Key Laboratory of Psychotic Disorders (13dz2260500); the Major Scientific Project of Zhejiang Lab (No. 2018DG0ZX01); the Fundamental Research Funds for the Central Universities (2019QNA5026, 2019XZZX001-01-08); and the Zhejiang University Education Foundation Global Partnership Fund.

Appendix A. Supplementary data

Supplementary data to this article can be found online at <https://doi.org/10.1016/j.neuroimage.2020.116906>.

References

- Alexander, D.C., 2008. A general framework for experiment design in diffusion MRI and its application in measuring direct tissue-microstructure features. *Magn. Reson. Med.* <https://doi.org/10.1002/mrm.21646>.
- Alexander, D.C., Hubbard, P.L., Hall, M.G., Moore, E.A., Ptito, M., Parker, G.J.M., Dyrby, T.B., 2010. Orientationally invariant indices of axon diameter and density from diffusion MRI. *Neuroimage*. <https://doi.org/10.1016/j.neuroimage.2010.05.043>.
- Andersson, J.L.R., Graham, M.S., Zsoldos, E., Sotiropoulos, S.N., 2016. Incorporating outlier detection and replacement into a non-parametric framework for movement and distortion correction of diffusion MR images. *Neuroimage* 141, 556–572. <https://doi.org/10.1016/j.neuroimage.2016.06.058>.
- Andersson, J.L.R., Sotiropoulos, S.N., 2016. An integrated approach to correction for off-resonance effects and subject movement in diffusion MR imaging. *Neuroimage* 125, 1063–1078. <https://doi.org/10.1016/j.neuroimage.2015.10.019>.
- Assaf, Y., Basser, P.J., 2005. Composite hindered and restricted model of diffusion (CHARMED) MR imaging of the human brain. *Neuroimage*. <https://doi.org/10.1016/j.neuroimage.2005.03.042>.
- Benjamini, D., Basser, P.J., 2017. Magnetic resonance microdynamic imaging reveals distinct tissue microenvironments. *Neuroimage*. <https://doi.org/10.1016/j.neuroimage.2017.09.033>.
- Benjamini, D., Basser, P.J., 2016. Use of marginal distributions constrained optimization (MADCO) for accelerated 2D MRI relaxometry and diffusometry. *J. Magn. Reson.* <https://doi.org/10.1016/j.jmr.2016.08.004>.
- Billiet, T., Vandenbulcke, M., Mädler, B., Peeters, R., Dhollander, T., Zhang, H., Deprez, S., Van den Bergh, B.R.H., Sunaert, S., Emsell, L., 2015. Age-related microstructural differences quantified using myelin water imaging and advanced diffusion MRI. *Neurobiol. Aging*. <https://doi.org/10.1016/j.neurobiolaging.2015.02.029>.
- Bouyagoub, S., Dowell, N.G., Hurley, S.A., Wood, T.C., Cercignani, M., 2016. Overestimation of CSF fraction in NODDI: possible correction techniques and the effect on neurite density and orientation dispersion measures. In: 24th Annual Meeting of the International Society for Magnetic Resonance in Medicine. Singapore.

- Campbell, J.S.W., Leppert, I.R., Narayanan, S., Boudreau, M., Duval, T., Cohen-Adad, J., Pike, G.B., Stikov, N., 2018. Promise and pitfalls of g-ratio estimation with MRI. *Neuroimage*. <https://doi.org/10.1016/j.neuroimage.2017.08.038>.
- Chang, Y.S., Owen, J.P., Pojman, N.J., Thieu, T., Bukshpun, P., Wakahiro, M.L.J., Berman, J.I., Roberts, T.P.L., Nagarajan, S.S., Sherr, E.H., Mukherjee, P., 2015. White matter changes of neurite density and fiber orientation dispersion during human brain maturation. *PLoS One*. <https://doi.org/10.1371/journal.pone.0123656>.
- Churchill, N.W., Caverzasi, E., Graham, S.J., Hutchison, M.G., Schweizer, T.A., 2017. White matter microstructure in athletes with a history of concussion: comparing diffusion tensor imaging (DTI) and neurite orientation dispersion and density imaging (NODDI). *Hum. Brain Mapp.* <https://doi.org/10.1002/hbm.23658>.
- Coleman, T.F., Li, Y., 1996. An interior trust region approach for nonlinear minimization subject to bounds. *SIAM J. Optim.* <https://doi.org/10.1137/0806023>.
- Cox, S.R., Ritchie, S.J., Tucker-Drob, E.M., Liewald, D.C., Hagenaars, S.P., Davies, G., Wardlaw, J.M., Gale, C.R., Bastin, M.E., Deary, I.J., 2016. Ageing and brain white matter structure in 3,513 UK Biobank participants. *Nat. Commun.* <https://doi.org/10.1038/ncomms13629>.
- Daducci, A., Canales-Rodríguez, E.J., Zhang, H., Dyrby, T.B., Alexander, D.C., Thiran, J.P., 2015. Accelerated microstructure imaging via convex optimization (AMICO) from diffusion MRI data. *Neuroimage*. <https://doi.org/10.1016/j.neuroimage.2014.10.026>.
- De Santis, S., Assaf, Y., Jeurissen, B., Jones, D.K., Roebroeck, A., 2016a. T1 relaxometry of crossing fibres in the human brain. *Neuroimage*. <https://doi.org/10.1016/j.neuroimage.2016.07.037>.
- De Santis, S., Assaf, Y., Jones, D.K., 2016b. The influence of t2 relaxation in measuring the restricted volume fraction in diffusion MRI. In: 24th Annual Meeting of the International Society for Magnetic Resonance in Medicine. Singapore.
- Dean, D.C., O'Muircheartaigh, J., Dirks, H., Travers, B.G., Adluru, N., Alexander, A.L., Deoni, S.C.L., 2016. Mapping an index of the myelin g-ratio in infants using magnetic resonance imaging. *Neuroimage*. <https://doi.org/10.1016/j.neuroimage.2016.02.040>.
- Desikan, R.S., Ségonne, F., Fischl, B., Quinn, B.T., Dickerson, B.C., Blacker, D., Buckner, R.L., Dale, A.M., Maguire, R.P., Hyman, B.T., Albert, M.S., Killiany, R.J., 2006. An automated labeling system for subdividing the human cerebral cortex on MRI scans into gyral based regions of interest. *Neuroimage*. <https://doi.org/10.1016/j.neuroimage.2006.01.021>.
- Ding, X.Q., Kucinski, T., Wittkugel, O., Goebell, E., Grzyska, U., Görg, M., Kohlschütter, A., Zeumer, H., 2004. Normal brain maturation characterized with age-related T2 relaxation times: an attempt to develop a quantitative imaging measure for clinical use. *Invest. Radiol.* <https://doi.org/10.1097/00004424-200412000-00005>.
- Fieremans, E., Burcaw, L.M., Lee, H.H., Lemberskiy, G., Veraart, J., Novikov, D.S., 2016. In vivo observation and biophysical interpretation of time-dependent diffusion in human white matter. *Neuroimage*. <https://doi.org/10.1016/j.neuroimage.2016.01.018>.
- Fu, X., Shrestha, S., Sun, M., Wu, Q., Luo, Y., Zhang, X., Yin, J., Ni, H., 2019. Microstructural white matter alterations in mild cognitive impairment and Alzheimer's disease: study based on neurite orientation dispersion and density imaging (NODDI). *Clin. Neuroimaging*. <https://doi.org/10.1007/s00062-019-00805-0>.
- Geeraert, B.L., Lebel, R.M., Lebel, C., 2019. A multiparametric analysis of white matter maturation during late childhood and adolescence. *Hum. Brain Mapp.* <https://doi.org/10.1002/hbm.24706>.
- Gibbons, E.K., Hodgson, K.K., Chaudhari, A.S., Richards, L.G., Majersik, J.J., Adluru, G., DiBella, E.V.R., 2019. Simultaneous NODDI and GFA parameter map generation from subsampled q-space imaging using deep learning. *Magn. Reson. Med.* <https://doi.org/10.1002/mrm.27568>.
- Golkov, V., Dosovitskiy, A., Sperl, J.L., Menzel, M.I., Czisch, M., Sämann, P., Brox, T., Cremers, D., 2016. q-Space deep learning: twelve-fold shorter and model-free diffusion MRI scans. *IEEE Trans. Med. Imag.* 35, 1344–1351.
- Graham, S.J., Stanchev, P.L., Bronskill, M.J., 1996. Criteria for analysis of multicomponent tissue T2 relaxation data. *Magn. Reson. Med.* <https://doi.org/10.1002/mrm.1910350315>.
- Grussu, F., Schneider, T., Tur, C., Yates, R.L., Tachrount, M., Ianuș, A., Yiannakas, M.C., Newcombe, J., Zhang, H., Alexander, D.C., DeLuca, G.C., Gandini Wheeler-Kingshott, C.A.M., 2017. Neurite dispersion: a new marker of multiple sclerosis spinal cord pathology? *Ann. Clin. Transl. Neurol.* <https://doi.org/10.1002/acn3.445>.
- Guerrero, J.M., Adluru, N., Bendlin, B.B., Goldsmith, H.H., Schaefer, S.M., Davidson, R.J., Keckemeti, S.R., Zhang, H., Alexander, A.L., 2019. Optimizing the intrinsic parallel diffusivity in NODDI: an extensive empirical evaluation. *PLoS One*. <https://doi.org/10.1371/journal.pone.0217118>.
- Jespersen, S.N., Kroenke, C.D., Østergaard, L., Ackerman, J.J.H., Yablonskiy, D.A., 2007. Modeling dendrite density from magnetic resonance diffusion measurements. *Neuroimage*. <https://doi.org/10.1016/j.neuroimage.2006.10.037>.
- Jung, W., Lee, Jingu, Shin, H.G., Nam, Y., Zhang, H., Oh, S.H., Lee, Jongho, 2018. Whole brain g-ratio mapping using myelin water imaging (MWI) and neurite orientation dispersion and density imaging (NODDI). *Neuroimage*. <https://doi.org/10.1016/j.neuroimage.2017.09.053>.
- Kamagata, K., Hatano, T., Okuzumi, A., Motoi, Y., Abe, O., Shimoji, K., Kamiya, K., Suzuki, M., Hori, M., Kumamaru, K.K., Hattori, N., Aoki, S., 2016. Neurite orientation dispersion and density imaging in the substantia nigra in idiopathic Parkinson disease. *Eur. Radiol.* <https://doi.org/10.1007/s00330-015-4066-8>.
- Kansagra, A.P., Mabray, M.C., Ferriero, D.M., Barkovich, A.J., Xu, D., Hess, C.P., 2016. Microstructural maturation of white matter tracts in encephalopathic neonates. *Clin. Imag.* <https://doi.org/10.1016/j.clinimag.2016.05.009>.
- Kim, D., Doyle, E.K., Wisnowski, J.L., Kim, J.H., Haldar, J.P., 2017. Diffusion-relaxation correlation spectroscopic imaging: a multidimensional approach for probing microstructure. *Magn. Reson. Med.* <https://doi.org/10.1002/mrm.26629>.

- Kodiweera, C., Alexander, A.L., Harezlak, J., McAllister, T.W., Wu, Y.C., 2016. Age effects and sex differences in human brain white matter of young to middle-aged adults: a DTI, NODDI, and q-space study. *Neuroimage*. <https://doi.org/10.1016/j.neuroimage.2015.12.033>.
- Kumar, R., Delshad, S., Woo, M.A., MacEly, P.M., Harper, R.M., 2012. Age-related regional brain T2-relaxation changes in healthy adults. *J. Magn. Reson. Imag.* <https://doi.org/10.1002/jmri.22831>.
- Kunz, N., Zhang, H., Vasung, L., O'Brien, K.R., Assaf, Y., Lazeyras, F., Alexander, D.C., Hüppi, P.S., 2014. Assessing white matter microstructure of the newborn with multi-shell diffusion MRI and biophysical compartment models. *Neuroimage*. <https://doi.org/10.1016/j.neuroimage.2014.03.057>.
- Lampinen, B., Szczepankiewicz, F., Novén, M., van Westen, D., Hansson, O., Englund, E., Mårtensson, J., Westin, C.F., Nilsson, M., 2019. Searching for the neurite density with diffusion MRI: challenges for biophysical modeling. *Hum. Brain Mapp.* <https://doi.org/10.1002/hbm.24542>.
- Lee, S.M., Choi, Y.H., You, S.K., Lee, W.K., Kim, W.H., Kim, H.J., Lee, S.Y., Cheon, H., 2018. Age-related changes in tissue value properties in children: simultaneous quantification of relaxation times and proton density using synthetic magnetic resonance imaging. *Invest. Radiol.* <https://doi.org/10.1097//RLI.0000000000000435>.
- Li, Z., Gong, T., Lin, Z., He, H., Tong, Q., Li, C., Sun, Y., Yu, F., Zhong, J., 2019. Fast and robust diffusion kurtosis parametric mapping using a three-dimensional convolutional neural network. *IEEE Access*. <https://doi.org/10.1109/ACCESS.2019.2919241>, 1–1.
- Lin, M., He, H., Tong, Q., Ding, Q., Yan, X., Feiwei, T., Zhong, J., 2018. Effect of myelin water exchange on DTI-derived parameters in diffusion MRI: elucidation of TE dependence. *Magn. Reson. Med.* <https://doi.org/10.1002/mrm.26812>.
- Lin, Z., Gong, T., Wang, K., Li, Z., He, H., Tong, Q., Yu, F., Zhong, J., 2019. Fast learning of fiber orientation distribution function for MR tractography using convolutional neural network. *Med. Phys.* <https://doi.org/10.1002/mp.13555>.
- MacKay, A., Laule, C., Vavasour, I., Bjarnason, T., Kolind, S., Mäder, B., 2006. Insights into brain microstructure from the T2 distribution. *Magn. Reson. Imaging*. <https://doi.org/10.1016/j.mri.2005.12.037>.
- MacKay, A.L., Laule, C., 2016. Magnetic resonance of myelin water: an in vivo marker for myelin. *Brain Plast.* <https://doi.org/10.3233/bpl-160033>.
- Mah, A., Geeraert, B., Lebel, C., 2017. Detailing neuroanatomical development in late childhood and early adolescence using NODDI. *PLoS One*. <https://doi.org/10.1371/journal.pone.0182340>.
- McKinnon, E.T., Jensen, J.H., 2019. Measuring intra-axonal T2 in white matter with direction-averaged diffusion MRI. *Magn. Reson. Med.* <https://doi.org/10.1002/mrm.27617>.
- Merluzzi, A.P., Dean, D.C., Adluru, N., Suryawanshi, G.S., Okonkwo, O.C., Oh, J.M., Hermann, B.P., Sager, M.A., Asthana, S., Zhang, H., Johnson, S.C., Alexander, A.L., Bendlin, B.B., 2016. Age-dependent differences in brain tissue microstructure assessed with neurite orientation dispersion and density imaging. *Neurobiol. Aging*. <https://doi.org/10.1016/j.neurobiolaging.2016.03.026>.
- Mori, S., Wakana, S., Van Zijl, P.C., Nagae-Poetscher, L.M., 2005. *MRI atlas of human white matter*. Elsevier.
- Nazeri, X., Chakravart, M., Rotenberg, D.J., Rajji, T.K., Rathi, X., Michailovich, O.V., Voineskos, A.N., 2015. Functional consequences of neurite orientation dispersion and density in humans across the adult lifespan. *J. Neurosci.* <https://doi.org/10.1523/JNEUROSCI.3979-14.2015>.
- Novikov, D.S., Veraart, J., Jelescu, I.O., Fieremans, E., 2018. Rotationally-invariant mapping of scalar and orientational metrics of neuronal microstructure with diffusion MRI. *Neuroimage*. <https://doi.org/10.1016/j.neuroimage.2018.03.006>.
- Pas, K., Komlos, M.E., Perl, D.P., Bassar, P.J., Benjamini, D., 2020. Retaining information from multidimensional correlation MRI using a spectral regions of interest generator. *Sci. Rep.* <https://doi.org/10.1038/s41598-020-60092-5>.
- Peled, S., Cory, D.G., Raymond, S.A., Kirschner, D.A., Jolesz, F.A., 1999. Water diffusion, T2, and compartmentation in frog sciatic nerve. *Magn. Reson. Med.* [https://doi.org/10.1002/\(SICI\)1522-2594\(199911\)42:5<911::AID-MRM11>3.0.CO;2-J](https://doi.org/10.1002/(SICI)1522-2594(199911)42:5<911::AID-MRM11>3.0.CO;2-J).
- Qin, W., Yu, C.S., Zhang, F., Du, X.Y., Jiang, H., Yan, Y.X., Li, K.C., 2009. Effects of echo time on diffusion quantification of brain white matter at 1.5T and 3.0T. *Magn. Reson. Med.* <https://doi.org/10.1002/mrm.21920>.
- Rae, C.L., Davies, G., Garfinkel, S.N., Gabel, M.C., Dowell, N.G., Cercignani, M., Seth, A.K., Greenwood, K.E., Medford, N., Critchley, H.D., 2017. Deficits in neurite density underlie white matter structure abnormalities in first-episode psychosis. *Biol. Psychiatr.* <https://doi.org/10.1016/j.biopsych.2017.02.008>.
- Sarrazin, S., Poupon, C., Teillac, A., Mangin, J.F., Polosan, M., Favre, P., Laidi, C., D'Albis, M.A., Leboyer, M., Lledo, P.M., Henry, C., Houenou, J., 2019. Higher in vivo cortical intracellular volume fraction associated with lithium therapy in bipolar disorder: a multicenter noddi study. *Psychother. Psychosom.* <https://doi.org/10.1159/000498854>.
- Smith, S.M., Jenkinson, M., Woolrich, M.W., Beckmann, C.F., Behrens, T.E.J., Johansen-Berg, H., Bannister, P.R., De Luca, M., Drobnjak, I., Flitney, D.E., Niazy, R.K., Saunders, J., Vickers, J., Zhang, Y., De Stefano, N., Brady, J.M., Matthews, P.M., 2004. Advances in functional and structural MR image analysis and implementation as FSL. *NeuroImage*. <https://doi.org/10.1016/j.neuroimage.2004.07.051>.
- Stikov, N., Campbell, J.S.W., Stroh, T., Lavelée, M., Frey, S., Novek, J., Nuara, S., Ho, M.K., Bedell, B.J., Dougherty, R.F., Leppert, I.R., Boudreau, M., Narayanan, S., Duval, T., Cohen-Adad, J., Picard, P.A., Gasecka, A., Côté, D., Pike, G.B., 2015. In vivo histology of the myelin g-ratio with magnetic resonance imaging. *Neuroimage*. <https://doi.org/10.1016/j.neuroimage.2015.05.023>.
- Tariq, M., Schneider, T., Alexander, D.C., Gandini Wheeler-Kingshott, C.A., Zhang, H., 2016. Bingham-NODDI: mapping anisotropic orientation dispersion of neurites using diffusion MRI. *Neuroimage*. <https://doi.org/10.1016/j.neuroimage.2016.01.046>.
- Veraart, J., Fieremans, E., Novikov, D.S., 2016. Diffusion MRI noise mapping using random matrix theory. *Magn. Reson. Med.* 76, 1582–1593. <https://doi.org/10.1002/mrm.26059>.
- Veraart, J., Novikov, D.S., Fieremans, E., 2018. TE dependent Diffusion Imaging (TEdDI) distinguishes between compartmental T2 relaxation times. *Neuroimage*. <https://doi.org/10.1016/j.neuroimage.2017.09.030>.
- Wachowicz, K., Snyder, R.E., 2002. Assignment of the T2 components of amphibian peripheral nerve to their microanatomical compartments. *Magn. Reson. Med.* <https://doi.org/10.1002/mrm.10053>.
- Whittall, K.P., MacKay, A.L., Graeb, D.A., Nugent, R.A., Li, D.K.B., Paty, D.W., 1997. In vivo measurement of T2 distributions and water contents in normal human brain. *Magn. Reson. Med.* <https://doi.org/10.1002/mrm.1910370107>.
- Zhang, H., Hubbard, P.L., Parker, G.J.M., Alexander, D.C., 2011. Axon diameter mapping in the presence of orientation dispersion with diffusion MRI. *Neuroimage*. <https://doi.org/10.1016/j.neuroimage.2011.01.084>.
- Zhang, H., Schneider, T., Wheeler-Kingshott, C.A., Alexander, D.C., 2012. NODDI: practical in vivo neurite orientation dispersion and density imaging of the human brain. *Neuroimage* 61, 1000–1016. <https://doi.org/10.1016/j.neuroimage.2012.03.072>.